Pyramid Crawler Design Report

Team Açaí e mi

Claudia Brunner, Jin Park, Ben Chuter, Wiley Webb

2016-02-12

Contents

1 Executive Summary

Our team aspired to create a small lego crawler that could ascend and descend a steep narrow shaft similar to those found inside the Egyptian pyramids. Our crawler successfully traversed the shaft in an efficient manner while carrying a bolt to simulate drilling capacity. After depressing a bumper switch at the top to turn on a light, it returned smoothly down the shaft. We prototyped various designs to determine a suitable gear ratio, driving wheel location, and stabilizing mechanisms to balance the friction and rolling forces.

Our final design, as shown in Figure 1, involved a two-sided folding frame. It used a pair of rubber bands to exert the necessary normal force on the shaft walls to maintain a suitable friction force that could allow it to descend and ascend without falling. Stretched to different lengths, these rubber bands provided a crucial moment on the crawler that predisposed it to climb in rather than out of the shaft. We used a gear ratio of 125:1 and ran the motor at 6V in ascent and 3V in descent to improve efficiency. On test day we used 13.99J in ascent and 1.40J in descent for a total of 15.39J, which was significantly below the 60J limit. We calculated that our motor was 53.0% efficient, our transmission was 34.7% efficient, and that our wheels were 89.1% efficient for a total experimental efficiency of 16.4%. To further reduce energy consumption and improve efficiency we could reduce the crawler weight.

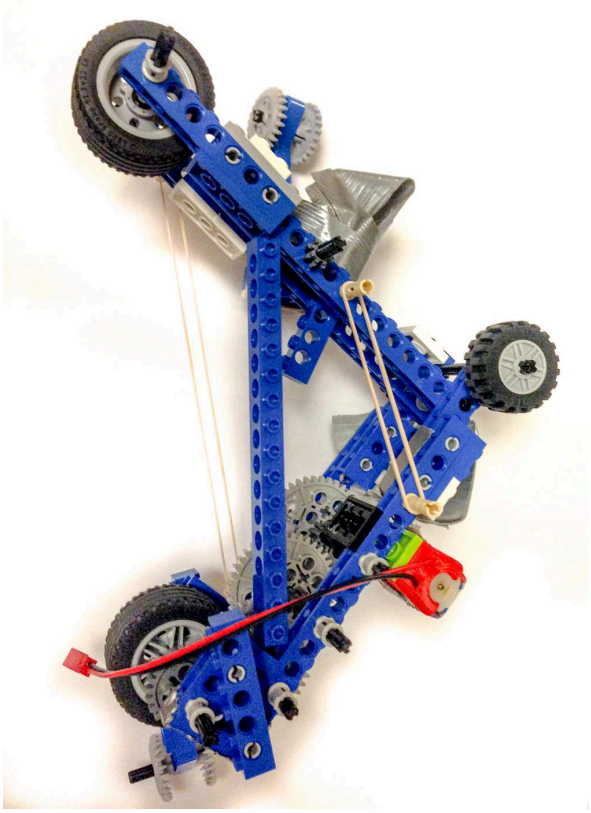

Figure 1: Crawler Design.

2 Background

Inspired by the recent discovery of a previously unknown chamber in an ancient Egyptian pyramid, we designed a crawler that could ascend a steep narrow shaft in order to explore the interior of the secret chamber. The shaft was 13.5 cm wide, 12.0 cm high, and angled at 60°. The motor could provide 3 to 6 Volts. The crawler would smoothly ascend the 2m shaft, while carrying a screw that would simulate a core drill. Then, the crawler would push a switch at the top of the shaft. Since littering is not permitted in pyramids, the crawler needed to descend the shaft again and not loose any parts during the process. We evaluated the crawler based on its reliability, energy efficiency, ability to carry the weight, and ability to press the switch at the top of the shaft. The energy efficiency of the crawler would be measured based on the power used over one meter up and down the shaft.

3 Basic Description of the Design

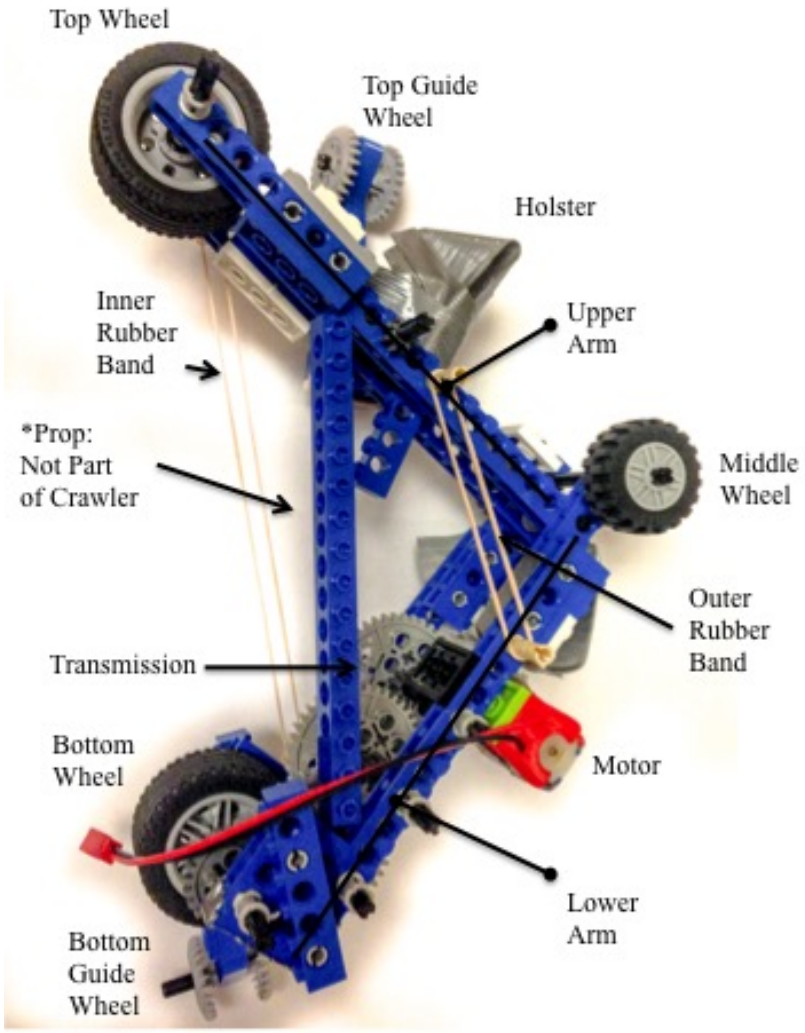

Figure 2: A figure labeling the different parts of the crawler as seen when placed inside the shaft. Side View.

The Frame We chose a 2-sided folding frame whose upper and lower arms could pivot relative to each other. This design established a normal force between the crawler and the shaft walls, since the crawler could be partially folded to be placed into the shaft. Once in the shaft, the rubber bands (connected between the opposing crawler arms) pulled the arms toward each other, establishing a normal force that allowed the crawler to move up the shaft due to the friction force (see Section 5). The frame arms had attachments that increased their overall length, past the length constraint of one long blue brick, since this prevents the crawler from wedging itself into the shaft (Appendices A.1, A.2, and A.3). Please see Appendices A.4 and A.5 for more detail.

Overall Transmission Ratio We chose an overall transmission ratio of 125 to provide the crawler with enough torque and drive force to overcome all negative forces that would prevent it from moving while not being over designed such that the crawler would move slowly and inefficiently. A transmission ratio of 125 gave an angular velocity that yielded relatively high efficiency and power values according to the respective curves and was not too distant from the maximum values (see Section 5). As such, the output forces of the motor could be greater than the sum of the negative forces of gravity $mg * cos(60°)$ and the internal and external resistances of the crawler. Thus, the crawler had enough torque to overcome difficult patches and yet was power efficient.

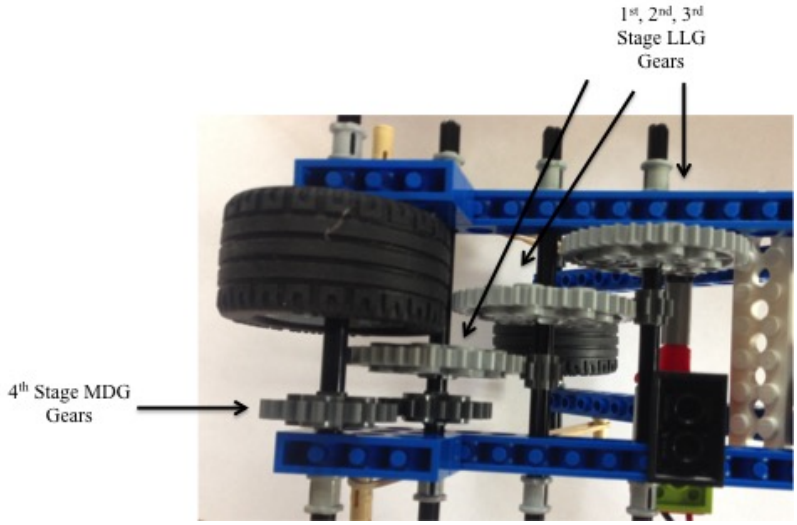

Figure 3: Chosen Transmission and Drive Wheel Arrangement. The three SDG to LLG shifts provided an overall 125 transmission ratio. Please note how the additional MDG gear on the power wheel axle did not exceed the circumference of the wheel. See Appendix Table A.1 for Abbreviation Legend.

Transmission Arrangement We opted to house the motor and transmission within the main frame to reduce any unnecessary system-unbalancing torque that could be caused by an externally-housed motor (Appendix A.6). Starting from the motor output side, three SDG to LLG shifts each provided a gear ratio of 5:1 for an overall ratio of 125:1 (see Appendix Table A.1. We found that smaller transmission ratios were less efficient and struggled to climb the shaft (Appendix A.7). By using the smallest and largest available gears we reduced the number of transmission stages while still achieving a sufficient gear ratio. We inserted a pair of MDG to MDG gears near the drive wheel so that the wheel would run freely without the gears that share its axle running against the shaft wall (Appendices A.8 and A.9).

Drive Wheel We chose one of the BR wheels in order to maximize the contact area between the wheel and the shaft wall. The rubber provided a high coefficient of friction so that the crawler could exert sufficient frictional force downward with minimal normal force. Minimizing the requisite normal force also decreased the rolling resistance and allowed more efficient movement.

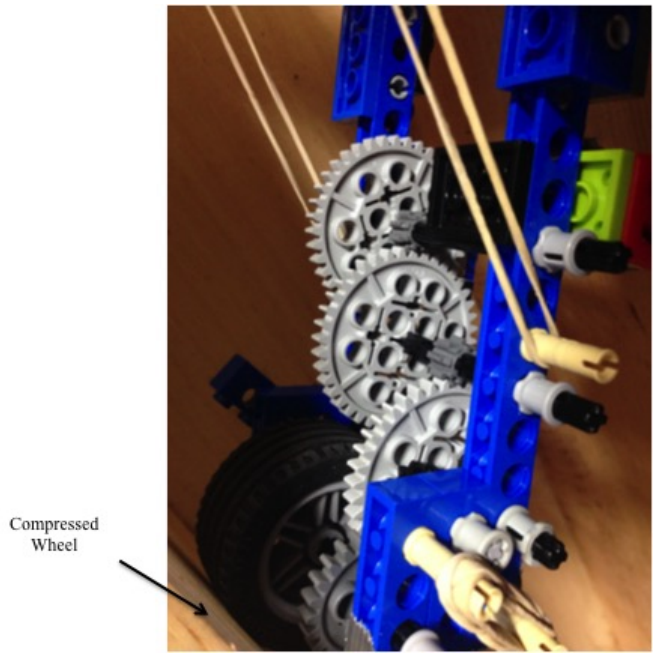

Figure 4: A close-up view of the drive wheel. Please observe the slight compression of the rubber wheel as the normal force presses it against the wall. Please also see above Figure 2 for overall crawler.

We positioned the wheel on the bottom side (closer to the ground) such that the crawler would be bottom-wheel driven as opposed to middle-wheel or top-wheel driven. This design choice took advantage of differences in dynamic and static normal forces among the different positions. If the drive wheel was in the top position, when the motor started and the drive wheel turned, the drive wheel initially pulled the top wheel arm up and off the shaft track, thus lowering the normal force and requiring greater static normal force from the rubber bands to keep it in place (Appendix A.10). However, if the drive wheel was in the bottom position, the opposite effect occurred. As it turned it instead pushed the bottom wheel arm up and into the shaft track, increasing the normal force and requiring less static normal force. The system was thus in effect self-energizing: the rotation of the drive wheel contributed to the normal force, increasing friction forces and allowing the crawler to drive up the shaft track. Placing the drive wheel in the middle position did not have this benefit.

We chose to have one drive wheel instead of two since there was little potential benefit from two drive wheels and greater risk. While two drive wheels could prevent slipping and require less overall normal force to function, increasing normal force was not an issue in our design. Furthermore, two transmission systems, if slightly misaligned, could cause differential gear ratios and thus establish a moment on the crawler forcing it out of the shaft or ramming it into the ground.

Stability Mechanisms: Guide Wheels, Rubber Bands, Bolt Positioning, and Dual Middle Wheels

Guide Wheels Guide wheels, mounted to run parallel to the direction of travel, stabilised the system and prevented the crawler from turning out of the shaft or running into the ground (Figure 2, Appendices A.4 and A.5). We constructed the final guide wheels from the LG24TW gears so that even if the arms shifted position and the axis of rotation was no longer perfectly perpendicular to the direction of motion the wheels, having a low coefficient of friction, could slide and still provide a sufficient normal force without excessive, counterproductive friction forces (Appendix A.11). Also, the kit provided four of these gears so that we could have wheels on both side of the guide wheel axle, which provided further stability, while other potential non-rubber wheels were only provided as a single pair of two in the kit (Appendix A.12). Finally, we cut the guide wheel axle to a shorter length, to prevent rubbing against the shaft wall if the wheel axle bent, yet not so short that the guide wheels were in danger of coming off the ends.

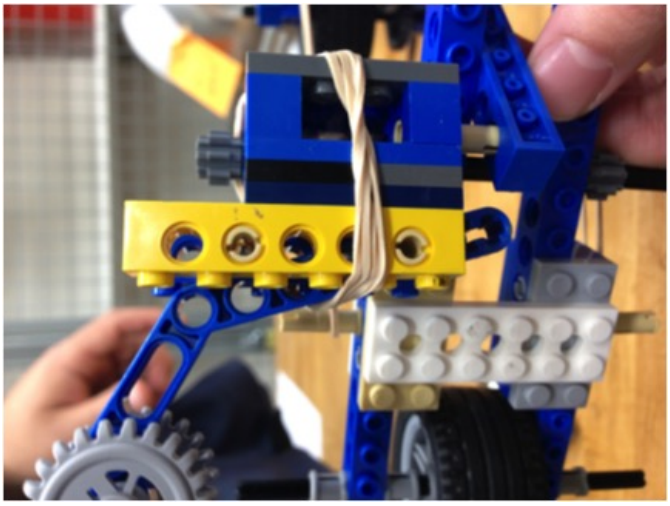

Figure 5: Close-up view of the auxiliary framework holding guide wheel system onto the main frame.

The guide wheel auxiliary frames to the main frame came under significant stress during ascent. To strengthen their connections, we used a rubber band and tape to hold the Legos^{TM} together and prevent them from becoming unstuck.

Rubber Bands Despite the guide wheels, our crawler tended to move up and out of the shaft, likely due to a moment resulting from the positioning of the drive wheel off the center of gravity. To address this, we created a counter-moment with our rubber bands. By being stretched to different lengths, they thus created a moment that canceled out the drive positioning moment (Appendix A.13). This change predisposed the crawler to run slightly against the inside of the shaft. However, that posed no significant issue because the crawler?s guide wheels provided a normal force, keeping it from running itself aground. We favored this inward-moving tendency since it meant that the crawler would not shift up and out, which was a problem we did not design an effective back-up mechanism for. Thus, the rubber bands allowed the crawler to ascend and descend reliably while staying in the shaft.

To further stabilize the crawler in the shaft, we used two rubber middle wheels to resist any moments that might be forcing them to run in or out of the shaft. We also added another axle around which the crawler folded, so that the wheel axle was separate and could rotate more freely, lowering friction and increasing efficiency.

Finally, we moved the bolt "core drill" holster, and thus the bolt too, to the inside part of the guide wheel (Figure 6 A)). This weight exerted another small force and thus moment keeping the crawler running along the inside of the shaft.

Core Drill We created a holster out of duct tape that allowed us to insert and remove the bolt from the crawler quickly and easily. This duct tape holster allowed us to save our Legos^{TM} for other parts of our crawler while also lowering the overall weight of the crawler.

Figure 6: A) Filled Holster. B). Unfilled Holster.

The Switch Depression Mechanism Our crawler depressed the switch at the top of the pyramid shaft by simply running into the switch with its top wheel. The use of the wheel, instead of an additional arm, allowed us to conserve our Legos^{TM} and keep the weight down, which improved the crawler's efficiency.

Descent Mechanism After depressing the switch, we simply reversed the leads so that the motor ran the opposite way. Since the tangential component of gravity was now propelling the crawler instead of acting against it, we also run the motor at 3V in descent instead of the 6V that we used to ascend. This voltage decrease let the crawler run at a safe, efficient speed.

4 Basic Description of the Logistics

To install the bolt, we placed the bolt in a duct tape holster that quickly but consistently secured it to the crawler. The frame was then partially folded and placed in the shaft. Once in the shaft, the pull of the rubber bands created a normal force that enabled the crawler to remain in the shaft without sliding. We then connected the motor to a power source, starting the system. The bottom drive wheel exerted a tangential frictional force, and with a 125 transmission ratio, the crawler had enough torque to overcome resistive forces and move up the shaft and yet was power efficient at 6V. As the crawler ascended, the guide wheels stabilized the crawler with a consistent normal force so that it stayed in the track. Upon reaching the top, the crawler activated the bumper switch by pushing its top wheel against the bumper switch.

After depressing the switch, we reversed the leads to run the motor in reverse. Since the tangential component of gravity was now accelerating the forward, we ran the motor at 3V so it still descended at a safe velocity. The crawler stayed in the track for the descent in the same way it did in the ascent. To stop at the bottom, we shut off the power, which caused the crawler to slow down and eventually halt altogether due to rolling resistance and internal friction. Since our crawler was relatively long and had rubber wheels with significant normal force pushing against the sides, it resisted the rotation necessary for the horizontal transition. Our design thus could not consistently conquer the bonus horizontal section, even at 9V. We instead decided to focus on surmounting the vertical section consistently and efficiently.

5 Analysis of Performance in the Shaft

In our analysis of shaft performance, we have included the 3V downward data but will focus on analysing the 6V upward data in detail.

	Voltage(s)	Current(A)	Time(s)
Up	6.0	0.29	8.04
Down	3.0	0.05	9.33

Table 1: Experimental Results from our final Crawler performance.

Next, we analysed our overall performance using with these values and equations:

- Crawler Mass: 0.27 kg
- Distance = 1 m
- Input electrical power = $V * I$
- Velocity = $\frac{d}{t}$
- Energy Usage = $P * t$
- Output Propulsion Power = $mg * sin(60°) * v$
- Energy Output = $mg * sin(60°) * d$
- Efficiency = $\frac{Energy\ Output}{Energy\ Usage}$

	Power In (W)	Velocity (m/s)	Power Output (W)	Energy Usage (J)	Efficiency (%)
Up	1.74	0.25	0.29	13.99	16.4
Down	0.15	0.21	*0.03	1.40	*22.4

Table 2: High level Analysis of Test Day Performance.

*While the crawler is not doing any useful work on the way down, it does overcome the rolling resistance of 0.314N for 1m while consuming 1.40J. Thus, it has an "efficiency" of 22.4% on the way down.

We then analysed where Power went in our Crawler and why. A power flow diagram showed the transfer of power across the motor, transmission, and wheels, between the initial input electrical power and final output work in propulsion power.

In order to translate input electrical power into propelling the crawler forward, our power flow had 3 parts to it. Each part had a story behind its design, as you can see in Section 3, and some advantages and disadvantages, which we analysed here.

1. Motor
2. Transmission
3. Wheels

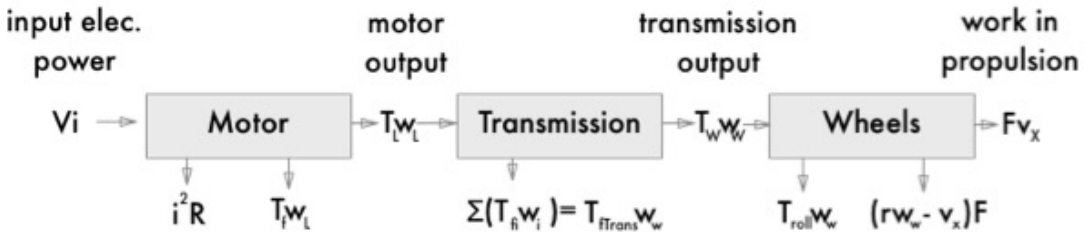

Figure 7: Power Flow Diagram.

Part 1: The Motor From characterising our motor via running No Load and Stall tests, we found it had these constants: $k = 0.004\ V/rad\ per\ sec$, $R = 8.4406\ \Omega$, and $T_F = 1.5853e{-}4\ Nm$. Because motor torque $= ki - T_F$, we plugged in our experimental Current values to find our corresponding angular velocity of the motor (Fig. 8), power output (Fig. 9), and efficiency (Fig. 10) for both the up and down trips.

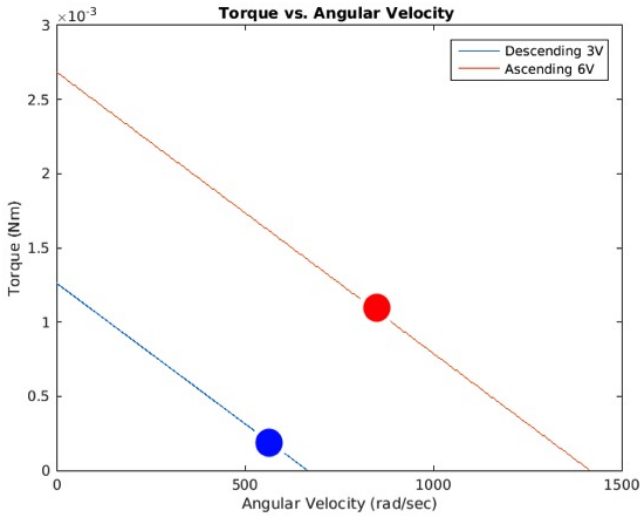

Figure 8: Torque vs. angular velocity during ascent and descent of the crawler.

We chose an angular velocity to run our motor that lies between peak Efficiency and peak Output power (Fig. 9 and 10),. This meant operating at a target current draw of around 0.275 A. On trial day our motor drew an input current of 0.29 A with a 6V input. Electrical power input into the motor equaled $VI = 1.74\ W$. On trial day, at 0.29 A of input current, our motor ran at 53% efficiency (Table 5 and 3). 47% of power was lost to internal motor resistance i^2R and motor friction $T_f\omega_L$. The remaining motor power output was $T_L\omega_L = 0.92\ W$.

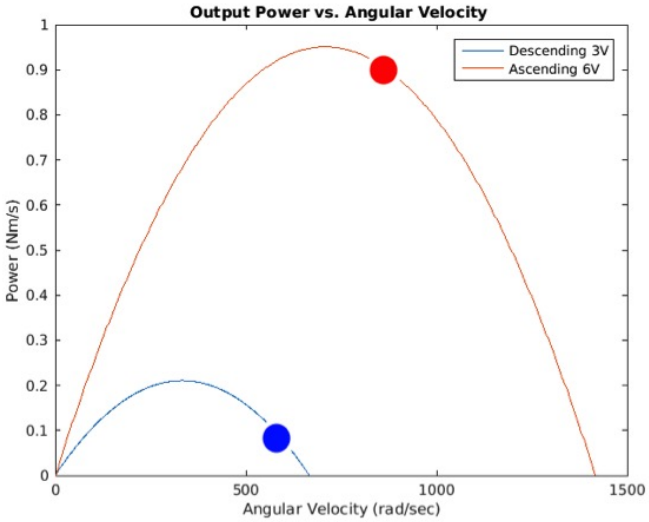

Figure 9: Output power vs. angular velocity during ascent and descent of the crawler.

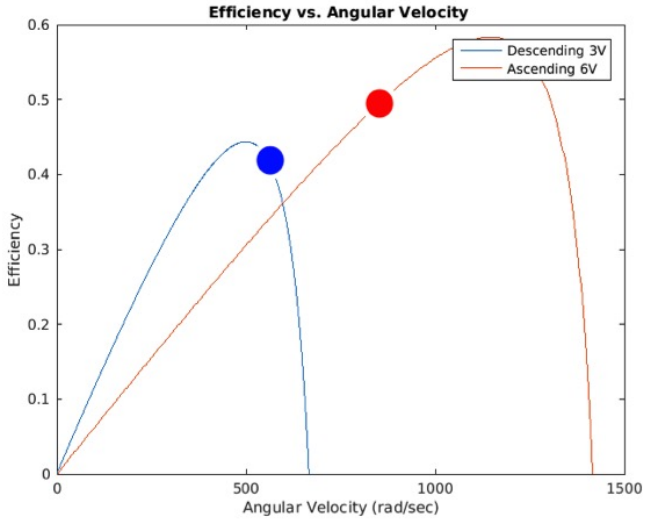

Figure 10: Efficiency vs. angular velocity during ascent and descent of the crawler.

	Torque ($Nm * 10^-3$)	Ang. Vel. (rad/s)	Power Out (W)	Effic. (%)
6V	1.2	820	0.90	53
3V	0.20	550	0.090	42

Table 3: Theoretical Motor Performance.

Part 2: Transmission Earlier in the week with the winch test, we measured our combined motor and transmission efficiency to be 19.9%. By dividing out our winch test motor effi-

ciency, which we also calculated to be 57.4% at an average current draw of .23A, we found our transmission efficiency to be 34.7%.

$$\text{Efficiency of Motor + Transmission} = \frac{mg*\Delta_y}{IV*t} = 19.9\%$$

$$\text{Efficiency of Transmission} = \frac{Motor+Transmission\ Efficiency}{Motor\ Efficiency} = 34.7\%$$

So, we lost 65.3% of power at this stage to internal frictions of the transmission between the gear teeth and between the axles and axle supports ($T_{F_{trans}}\omega_w$). The power delivered to the wheels is $19.9\% * 1.74\ W = 0.35\ W$.

Part 3: Wheels Finally, we analysed the wheels. A free body diagram helped us understand the forces acting upon our crawler.

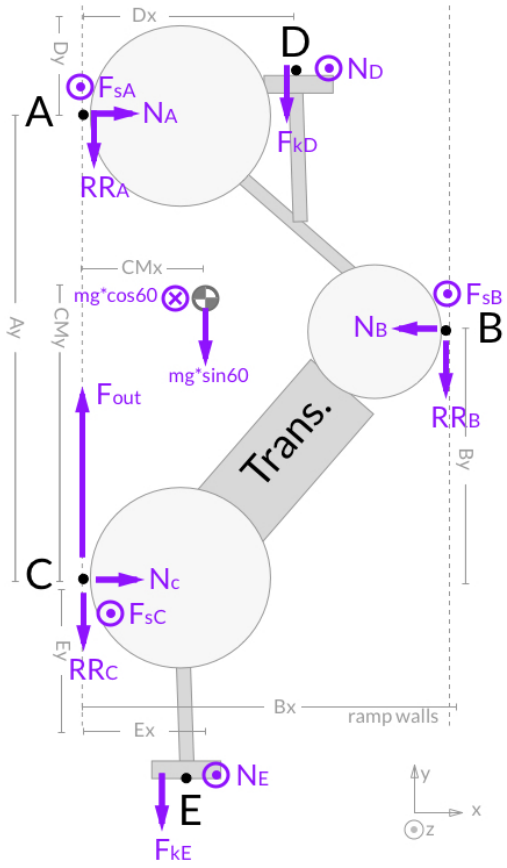

Figure 11: Free Body Diagram.

Here, the free body diagram (Fig. 11) is drawn with the plane of the page = the plane of the ramp. The forces are in purple and our crawler in grey. In the diagram, we used a circle with a dot to designate out of the page and a circle with an X for into the page.

Breakdown of forces:

- x
  - Na, Nb, and Nc = Normal forces from the walls on Wheel A, B, and C
- y
  - Fout = output power force from drive wheel C
  - $mg * sin(60°)$ = component of the total crawler weight
  - RRa, RRb, and RRc = Rolling resistance on Wheel A, B, and C
  - Fkd and Fke = Kinetic Friction forces from the floor on Support Arm D and E
- z
  - $mg * sin(60°)$ = component of the total crawler weight
  - Nd and Ne = Normal forces from the floor on Support Arm D and E
  - Fsa, Fsb, and Fsc = Static Friction forces from the walls on Wheel A, B, and C

Force Equations:

$$\sum F_y = 0 = F_{out} - RR_T - F_{S1} - RR_M - RR_B - F_{S2} - mg * cos(60°)$$

$$\sum F_x = 0 = N_T + N_B - N_M$$

$$\sum F_z = 0 = mg * sin(60°) - N_{S1} - N_{S2} - F_{SM} - F_{ST} - F_{SB}$$

Moment Equations:

$$\sum M_{z\ axis}^{all/C} = 0 = mg * cos(60°) * CM_x + RR_B * B_x + F_E * E_x + F_D * D_x + N_A * A_y - N_B * B_y$$

where $CM_x = 6$, $B_x = 14$, $E_x = 4$, $D_x = 6$, $B_y = 18$, $A_y = 28$

$$\sum M_{y\ axis}^{all/C} = 0 = -mg * sin(60°) * CM_x + N_D * D_x + F_SB * B_x + N_E * E_x$$

where $CM_x = 6$, $D_x = 6$, $E_x = 4$, $B_x = 14$

$$\sum M_{x\ axis}^{all/C} = 0 = -mg * sin(60°) * CM_y + F_SB * B_y + F_{SA} * A_y - N_E * E_y + N_D * D_y$$

where $CM_y =$, $B_y =$, $A_y =$, $E_y =$, $D_y =$

We found our rolling resistance by balancing the crawler on one side of the ramp with a bucket of sand on the other side. We then added sand to the bucket until the crawler started

rolling upwards at a constant velocity to determine our additional Rolling Resistance = 0.31N. This means that $0.314\ J = T_{Roll}\omega_w + (r\omega_w - vx)F$ worth of work went into rolling up the ramp.

Wheel Efficiency = $\frac{Overall\ Efficiency}{Motor+Transmission\ Efficiency} = \frac{16.4\%}{19.p\%} = 82.4\%$

Rolling Resistance Work = $0.032\ kg * 9.8\ m/s^2 * 1\ m = 0.314\ J = T_{Roll}\omega_w + (r\omega_w - vx)F$

Energy Going into Wheels = $V * i * t * (Motor + Transmission\ Efficiency) = 6\ V * 0.29\ A * 8.04\ s * .199 = 2.784\ J$ Expected Wheel Efficiency = $\frac{E_{in} - E_{lost}}{E_{in}} = \frac{2.784 - 0.314}{2.784} = 89.1\%$

Compared to the Expected Wheel Efficiency of 89.1% from the test performance values, the observed winch test wheel efficiency of 82.4% seems reasonable. Below, we double checked our results:

Check: $UsefulWorkDone = E_{in} * Motor\ Efficiency * Transmission\ Efficiency * Wheel\ Efficiency = 13.99 * 53.0 * 89.1 = 2.29J$
$Energy\ Out\ of\ Wheels = m * g * sin(60°) * d = .27 * 9.8 * sin(60°) * 1\ m = 2.29\ J$

For more detail on this derivation, please refer to our Energy Analysis Matlab Code (Appendix A.2).

6 Strength Estimate

As expected, the gears in the final stage of our system bore the greatest stress among those used in our transmission. For the stress estimate calculations, we assumed perfect transmission efficiency; actual stresses for the worst case gear(s) will be less than what we calculated. Given the operating conditions of the motor during the trial, we estimated the Lewis stresses on each of the gears in the final stage to be 2787.5 psi. [1] This is comfortably under the maximum stress for lego gears, which is 5000 psi. [2] As the two gears were identical in pitch (25.4) and teeth count (24 teeth), we estimated both gears in the final stage of our transmission to bear the same stress. Important factors that affected the strength of the gears included face width, material, and gear size. The greater the face width the stronger the gear as the stress was distributed, while stronger materials naturally allowed for stronger gears. Gear size was important as well since the involute profile for smaller gears cut into the base area and undermined the structural integrity of the gears. The anticipated loads come from the rolling resistance, as well as the component of gravitational force that affects the crawler. As calculated from the free body diagram, the combined gravitational and rolling resistance forces total to 2.6N, which is well below the estimated tangential force of 6.77N that is applied at the wheels of our crawler. Our transmission would be able to carry a crawler nearly three times its mass, making our design robust in achieving our goal of scaling the pyramid channel.

$$6.77N = Ftan_{wheel} > m_{crawler} * g * sin(60°) + m_{rolling} * g$$

Rearranging equations:

$$m_{crawler} < \frac{\frac{Ftan_{wheel}}{g} - 0.032g}{sin(60°)} = 763.5g$$

Please see Appendix Table A.3 for a tabulation of related forces and stresses for all gears and stages.

[1] MATLAB source code for calculations attached
[2] http://bdml.stanford.edu/Main/CrawlerNotes

7 Conclusions

All in all, our crawler performed very well, delivering replicable results through the final stages of testing. The crawler met no complications during the final trial demonstration, scaling the shaft on its first attempt. With a total energy usage of 15.39 Joules and a power efficiency of 16.4%, our crawler exhibited excellent performance. Throughout testing, our crawler demonstrated replicable results for scaling time and power consumption, as well as maintaining positioning and trajectory within the shaft. As expected, the crawler ascended the channel in roughly eight seconds, and never left the channel. Our crawler operated at a total efficiency of 16.4%, which is just slightly better than our calculated efficiency based on testing of our crawler. This could be due to slight differences in testing conditions, such as discrepancies in transmission lubrication. Another reason could be differences in the way the crawler was loaded between the winch test and trial day. Other differences could be due to errors in timing and measurements both during crawler specification tests and on trial day.

There are a number of ways in which we could improve the overall efficiency by changing the load of our crawler. To begin, our crawler was massive, weighing in at 270 grams. Redesigns to minimize mass and excess parts could decrease the load on the motor and transmission, reduce energy consumption, and improve overall efficiency. Another way would be to improve the efficiency of our transmission by lubricating additional moving parts of the crawler. While we lubricated our gears, future designs could benefit from lubricating shafts and axle bearings, which, on lego technic parts, have a significant degree of friction. Further design modifications to the current crawler design would include stabilization and alignment of the guide wheels. The guide wheels, while functional, were not entirely parallel with the track, which likely resulted in higher friction forces on the crawler than necessary. Improving guide wheel alignment would minimize friction and likely improve overall efficiency. Unnecessary loads as those described above indirectly decrease the transmission's overall efficiency, and efforts to reduce these loads would improve crawler performance.

Finally, under the current design, while the crawler is capable of constant ascent up a channel, it does poorly in case of a track with changing angles. If there are severe perturbations in the channel, such as significant debris or unexpected changes in the channel's trajectory, it is likely that our design will encounter complications. Should we redesign our crawler, we would change the axis about which our crawler would pivot in a way that allows more flexibility in adjusting the crawlers trajectory to meet changes in the shaft.

Assuming that the pyramid shaft is accurately modeled by the ME112 simulation track, our crawler will successfully and replicably complete pyramid exploration. All in all, this crawler meets the requirements of an unobstructed pyramid channel ascent in a timely and energy-efficient manner, and would be of great assistance in ancient artifact exploration.

A Appendices

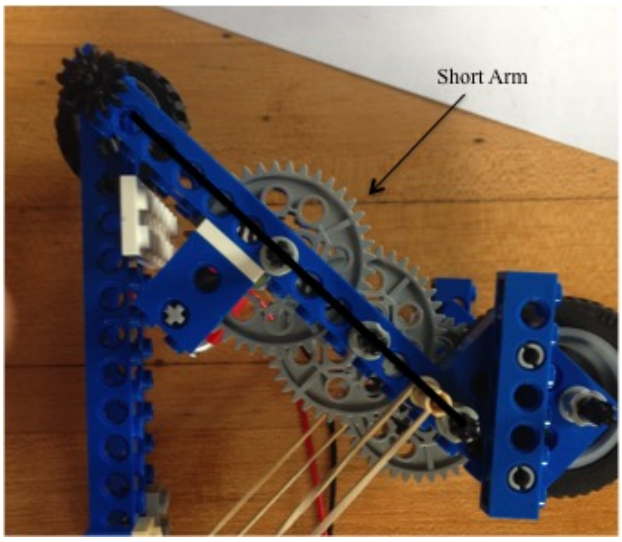

Figure A.1: The short arm on the drive motor arm.

A.1

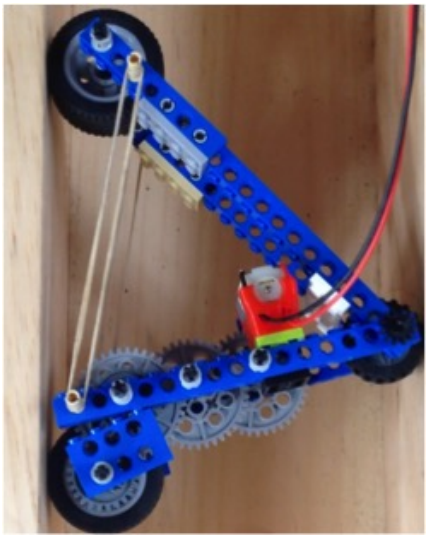

Figure A.2: With a short drive arm, the crawler wedges itself into the sides of the shaft. Please also note how the Lego axle connection has disconnected as a result of this increased stress. Note that we had already increased the opposing lever arm so that the rubber bands would stretch to increase the normal force and also so that the motor would fit when the crawler folded in the shaft.

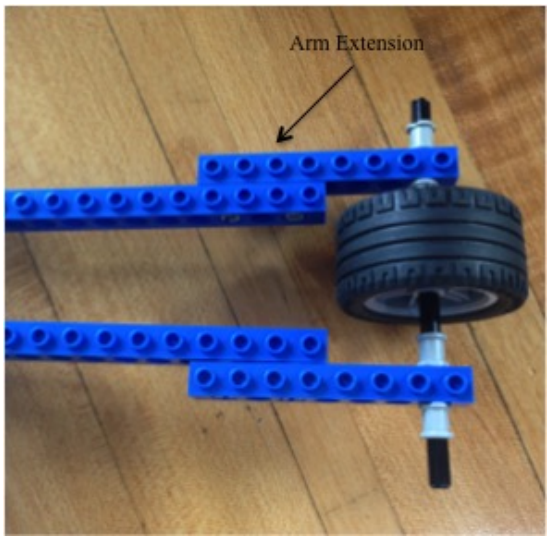

Figure A.3: The frame arms have extensions that increase their overall length past the constraint of one long blue brick since this prevents the crawler from wedging itself into the shaft.

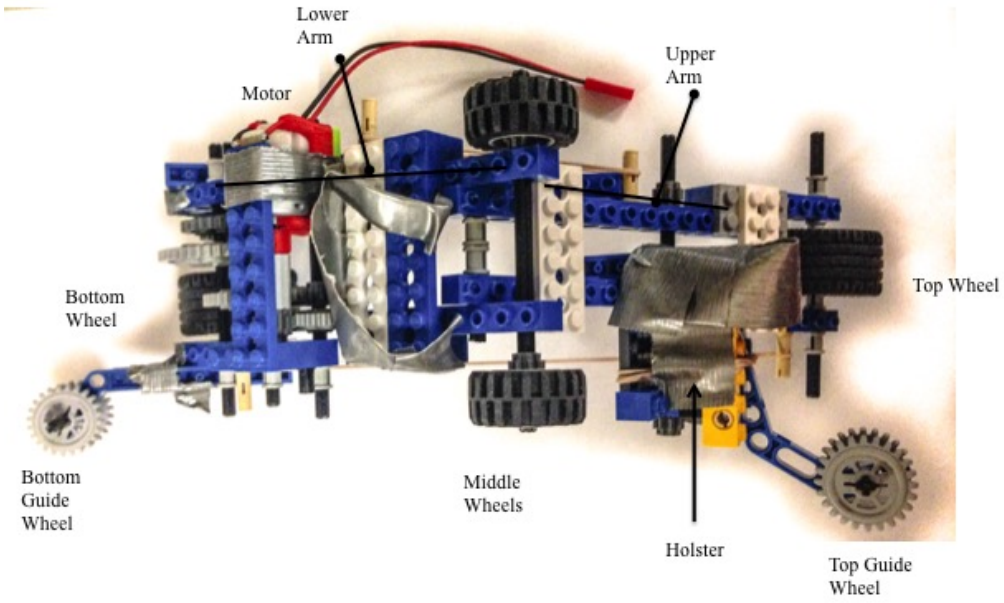

Figure A.4: A figure labeling the different parts of the crawler. View from the right interior side of the shaft.

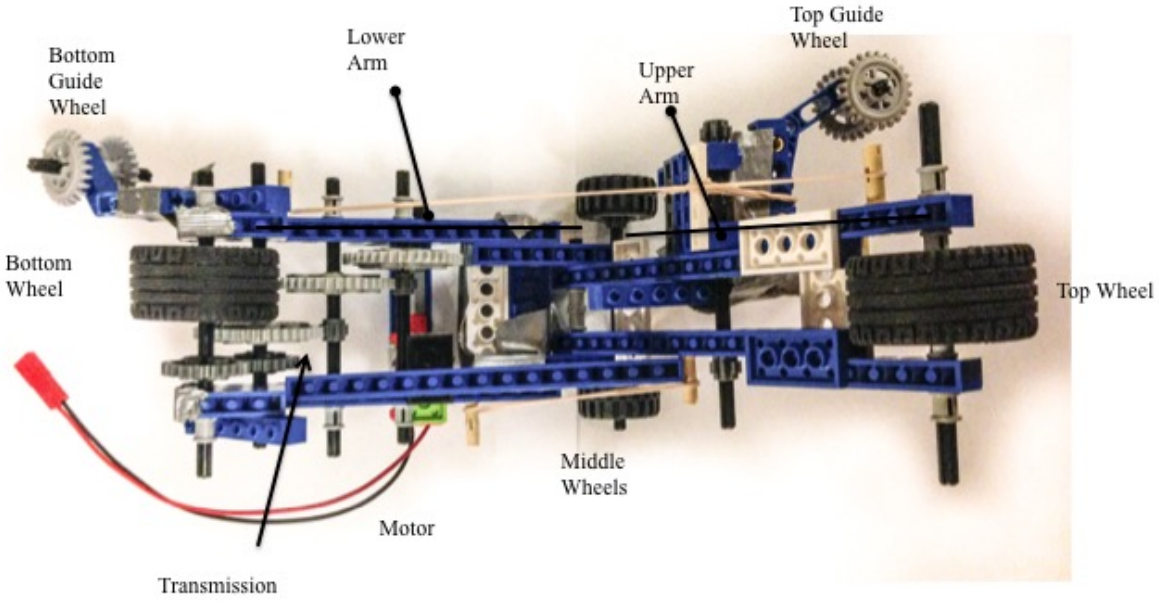

Figure A.5: A figure labeling the different parts of the crawler. View from the left interior side of the shaft.

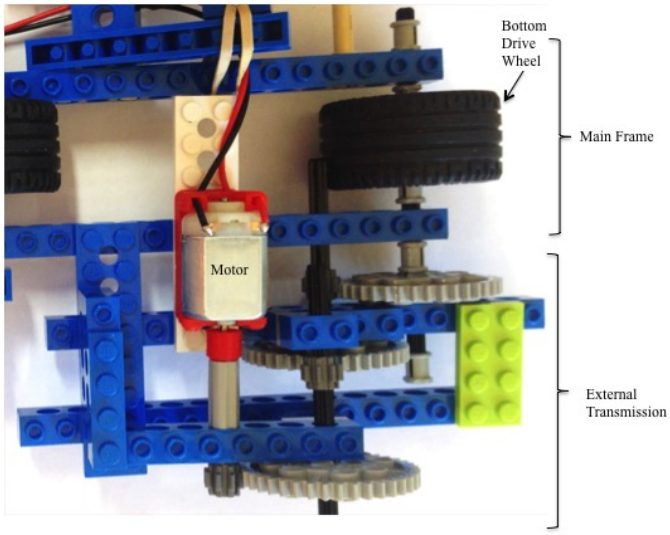

Figure A.6: An early prototype having an externally-housed motor that caused a system-unbalancing torque.

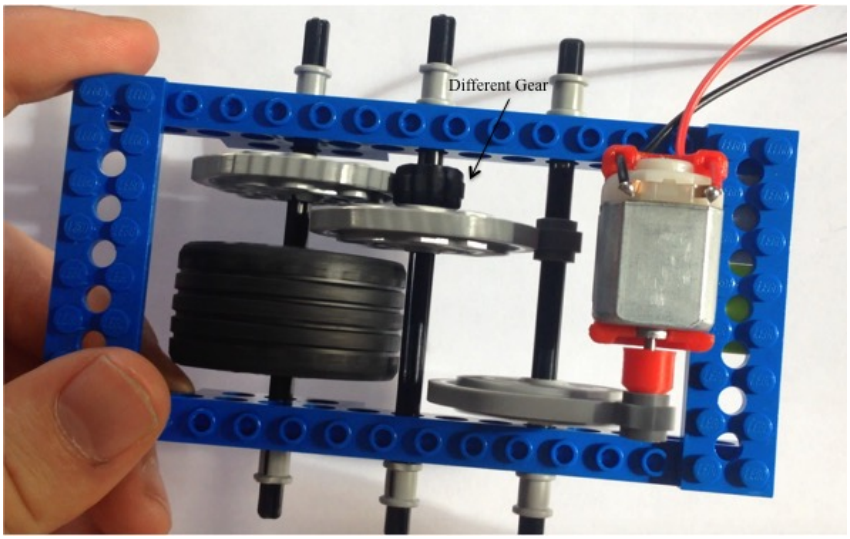

Figure A.7: An earlier transmission with a smaller overall ratio that was less efficient and weaker.

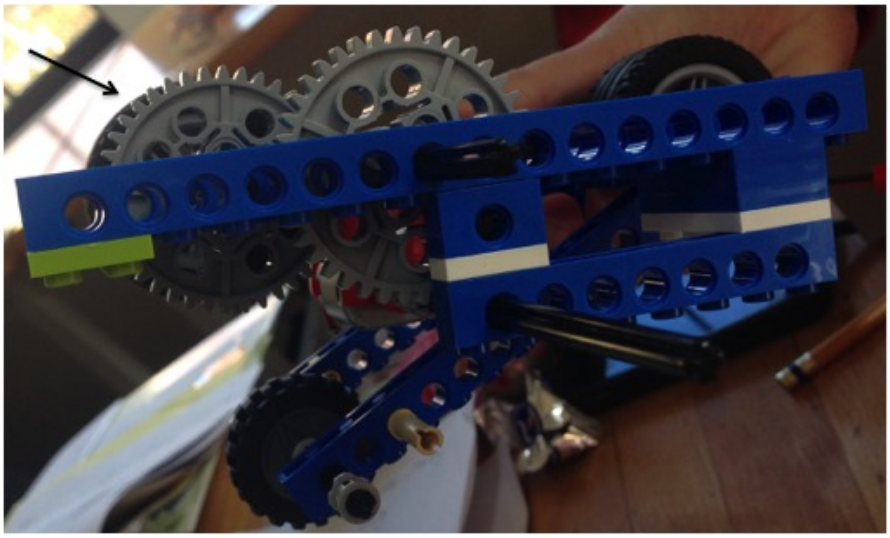

Figure A.8: Note how the LGG overlaps with the tire. When in the shaft, the tire compresses so that the gear instead takes most of the load. This gear loading decreases the coefficient of friction, thus requiring more normal force to provide sufficient force up the shaft. The additional forces on the gear teeth also wear them down faster and make them more liable to fail.

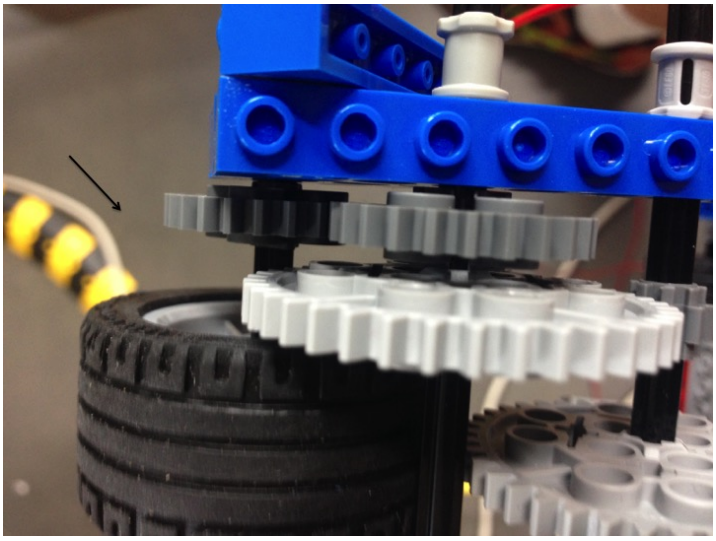

Figure A.9: With the addition of the fourth gear stage using two smaller MDG gears only wheel will be in contact with the shaft walls as desired.

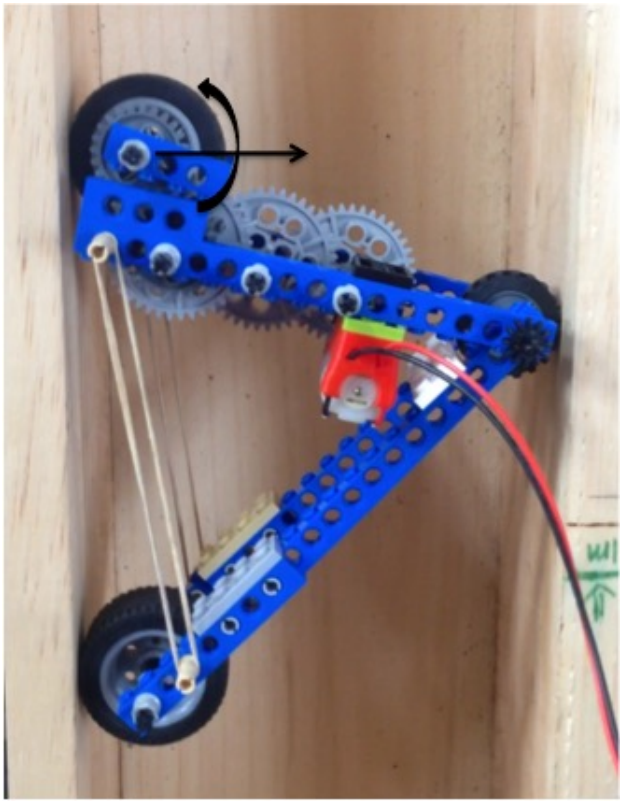

Figure A.10: When the motor starts and the drive wheel turns it initially pulls the top wheel arm up and off the shaft track, thus lowering the normal force and requiring greater static normal force from the rubber bands to keep it in place.

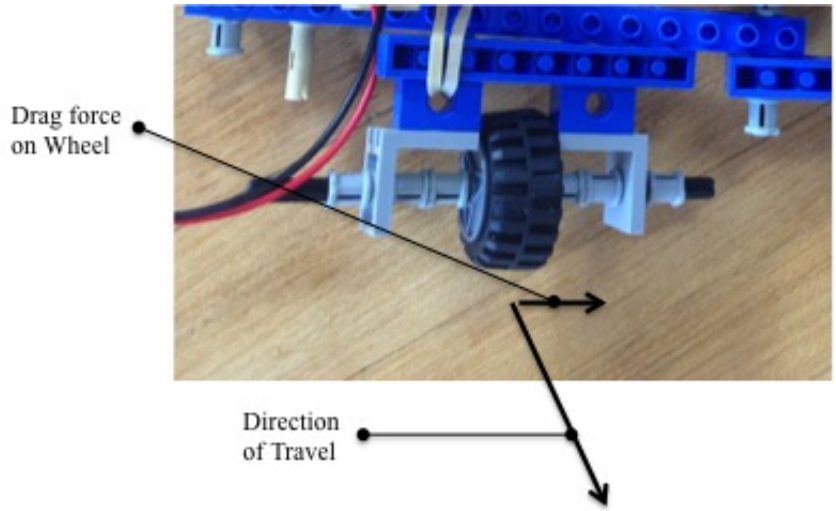

Figure A.11: This rubber guide wheel of an early prototype would catch and drag on the shaft if the wheel was not aligned perfectly with the direction of motion, radically decreasing efficiency.

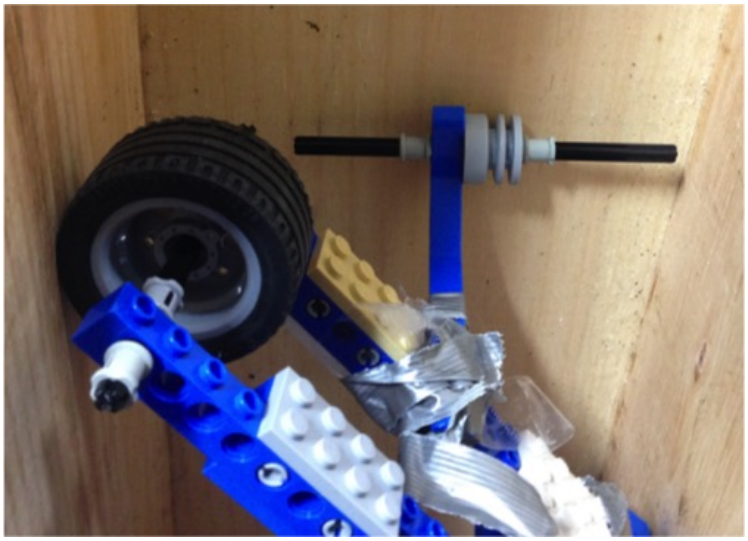

Figure A.12: The kit provided only two of these otherwise functional non-rubber wheels so that only one could be on the top and bottom guide wheel axles. Having only one wheel on each axle, however, created a moment that could bend the axle and cause it to rub on the shaft wall. As such, the spur gears, of which there were four, were chosen instead.

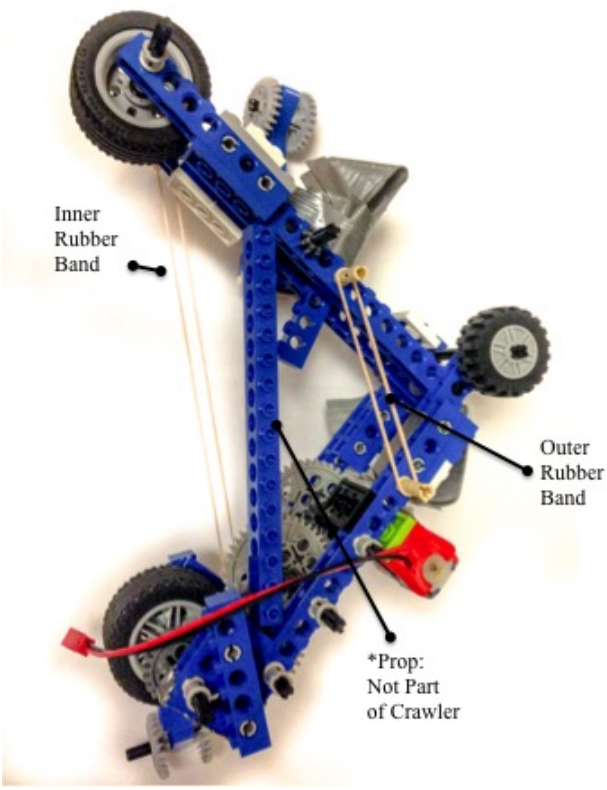

Figure A.13: To counteract our crawler's tendency to move up and out of the shaft, we created a counter-moment with our rubber bands by stretching them to different lengths.

Gear	Teeth
Large Light Gray (LLG) Gear	40
Medium Dark Gray (MDG) Gear	24
Small Dark Gray Gear (SDG)	8
Black Large Gear (BLG)	20
Black Small Gear (BSG)	12
Screw Worm Gear (SWG)	–
Light Gray Worm (LG24TW) Gear	24

Table A.1: Gear Types Abbreviations Legend.

Table A.2: Energy Analysis Matlab Code

This code does a basic energy balance of the crawler in the shaft. The values calculated at the end show the leftover energy output that is not consumed by inefficiencies in the motor, transmission, and in the final case, the rolling resistance.

```
V = 6;
i = .29;
t = 8.33;
AetaMotor = .574;
AetaMotorAndTrans = 0.199;
AetaTrans = AetaMotorAndTrans./AetaMotor
m = .27;
g = 9.8;
h = sin(degtorad(60));
R_roll = .3136;
E_roll = R_roll.*1;

EnergyLeftBeforeRollingLoss = (V*i*t*AetaMotorAndTrans)
EnergyLeftAfterRollingLoss = (V*i*t*AetaMotorAndTrans) - E_roll
WheelEfficiency = EnergyLeftAfterRollingLoss./EnergyLeftBeforeRollingLoss
```

Results: WheelEfficiency = 0.8910

Time (s)	V (Volts)	Current (A)	$\Delta_y(m)$	$P_{out}(W)$	$P_{in}(W)$	Motor+Trans. Effic.
8.35	6	0.23	0.84	0.266	1.38	0.193
8.20	6	0.25	0.8	0.258	1.50	0.172
8.46	6	0.20	0.89	0.279	1.2	0.237

Average motor + transmission efficiency: 13.8%

Table A.3: Winch Test Results.

		Teeth	Pitch	PD(in)	Ftan (lb*f)	Vtan (in/s)	Kv	Jlewis	Sigma_L (psi)
Stage 1	Gear 1	8	25.4	0.3150	0.0563	139.9	1.166	0.21	113.41
	Gear 2	40	25.4	1.5748				0.328	72.61
Stage 2	Gear 3	8	25.4	0.3150	0.2814	27.97	1.077	0.21	523.81
	Gear 4	40	25.4	1.5748				0.328	335.4
Stage 3	Gear 5	8	25.4	0.3150	1.4071	5.59	1.035	0.21	2516.8
	Gear 6	40	25.4	1.5748				0.328	1611.4
Stage 4	Gear 7	24	25.4	0.9449	2.3451	3.35	1.166	0.356	2787.5
	Gear 8	24	25.4	0.9449				0.356	2787.5

Table A.4: Gear Stress Table.